Spatial electroluminescence distribution and internal quantum efficiency in substrate free InAsSbP/InAsSb double heterostructure

© B.A. Matveev[1], V.I. Ratushnyi[2], A.Yu. Rybal'chenko[2]

[1] Ioffe Institute,
194021 St. Petersburg, Russia
[2] Volgodonsk Engineering and Technical Institute — branch of the National Research Nuclear University MEPhI,
347360 Volgodonsk, Russia

E-mail: bmat@iropt3.ioffe.ru

Received April 5, 2023
Revised July 26, 2023
Accepted August 1, 2023

In this work, we calculated the spatial distribution of the electroluminescence intensity taking into account the features of current spreading and taking into account the dependence of the internal quantum yield on the current density with the dominance of Auger recombination in flip-chip diodes based on InAsSbP/InAsSb double heterostructures ($\lambda = 4.2\,\mu$m). By comparing the calculated data and the radiation distribution over the sample surface, the internal quantum efficiency of electroluminescence and its dependence on the current density at room temperature are determined.

Keywords: $A^{III}B^{V}$ narrow gap heterostructures, mid-IR LEDs, current crowding in LEDs, InAsSb based LEDs, internal quantum efficiency in InAsSb based LEDs.

DOI: 10.61011/SC.2023.06.57172.4798

1. Introduction

Mid-infrared light emitting diodes and photodiodes (LED and PD, respectively) based on heterostructures (HS) InAsSbP/InAsSb are used in many industrially produced gas analyzers in demand for medicine, solving environmental problems and (or) production safety [1–3].

One of the features of a LED with contacts of a limited area, for example, a flip-chip LED, is the localization of current flow under the contacts and (or) in the immediate vicinity of them. When studying this localization, current density distribution $j(x, y)$ is usually modeled based on the solution of the Laplace equation, and the resulting distribution $j(x, y)$ is compared/corrected in accordance with the experimental distribution of electroluminescence intensity (EL) $L(x, y)$ [4,5]. At the same time, assumptions about the numerical relationship between $L(x, y)$ and $j(x, y)$ are usually not specified, in other words, a linear relationship between them is tacitly assumed: $L(x, y) \propto j(x, y)$ and it is assumed that there is an independence of the internal quantum efficiency of the EL (IQE, η_{int}) from the current. This assumption is valid only in the special case, which usually occurs only at small values of $j(x, y)$; in practice, this relationship is nonlinear mainly due to the fact that the rates of radiative and non-radiative recombination depend differently on the concentration of nonequilibrium charge carriers and, accordingly, on the current density $j(x, y)$.

In relation to mid-IR LED, the sublinearity of the dependence of the output power of the LED on the current has been discussed repeatedly; for example, in the work [6], an external quantum efficiency (EQE) was calculated with partial localization of current flow under a point opaque contact on the light-emitting surface of a model structure based on InAsSbP/InAs(Sb). At the same time, the calculations of the dependence of IQE on the local current density were not compared with the experiment.

In this paper, IQE estimates for various pumping currents are carried out, obtained by numerical analysis of the spatial distribution of the EL intensi in a flip-chip LED based on double heterostructures (DHS) InAsSbP/$InAsSb_{0.08}$ emitting at a wavelength of $\lambda_c = 4.2\,\mu$m.

2. Samples and measurement procedure

Epitaxial structures were grown on n^+-InAs substrates and contained an active region from an undoped solid solution n-$InAs_{0.92}Sb_{0.08}$ (band gap $E_g\,(300\,\text{K}) \sim 0.3\,\text{eV}$), enclosed between two wider-band layers of a quaternary solid solution InAsSbP, one of which was a contact layer p-InAsSbP(Zn).

The samples were made by standard photolithography in geometry for flip-chip mounting on specialized silicon circuit boards and were similar to those described in [7]. The emitting region of the flip-chip diode ($\lambda_c = 4.2\,\mu$m, FWHM $= 0.6\,\mu$m) had the form of a square mesa with a size of $220 \times 220\,\mu$m and a height of $7-8\,\mu$m; on its surface, i.e., on the p-InAsSbP layer, a wide square anode from a multilayer composition Cr-Au(Zn)-Ni-Au was formed by evaporation in vacuum. The rectangular cathode, made of a multilayer composition Cr-Au-Ni-Au, was located to the side of the mesa, as shown in Figure 1. „The active" part of the cathode, located on the surface of n-InAsSb and providing ohmic contact, had a size of $\sim 45 \times 200\,\mu$m, the distance from the edge of the cathode to the edge of

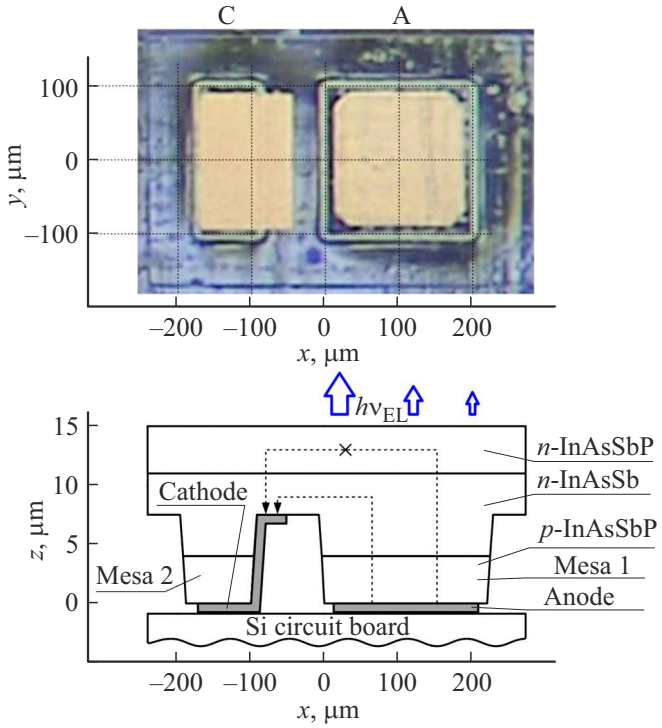

Figure 1. Photo of the chip surface from the contacts side (top) and the diode cross-section diagram (bottom). C — cathode; A — anode; Si circuit board — silicon circuit board; mesa 1 — main mesa with active, radiating region; mesa 2 — auxiliary mesa for connecting the layer of the *n*-type of conductivity to the cathode. The vertical arrows show the direction of movement of photons released from the semiconductor, generated during EL.

the mesa was $\ell_{c-m} \sim 45\,\mu$m. „The passive“ part of the cathode, located on the surface of the auxiliary mesa and partially on its slope, served for electrical connection with the conductive busbars of the circuit board. After soldering the chips onto the circuit boards, the substrate n^+-InAs was removed by chemical etching.

A description of the properties of a LED with a contact arrangement similar to that shown in Figure 1 can be found in many works discussing the localization of current flow and the accompanying distortions of the type of current-voltage ($I-V$) characteristics [4,5]. The path of current flow and the resulting distortion of the $I-V$ curve type are spatially uneven in the studied samples: the forward current was not described using the modified Shockley formula, but increased by power function with increasing voltage: $I \propto U^{1.4}$.

The distribution of the EL intensity over the surface of the diode mounted on the board when powered by direct current was recorded using an IR microscope with a cooled matrix detector of 128×128 elements based on InAs, having a maximum sensitivity at the wavelength of $\lambda \sim 2.9\,\mu$m and a sharp decrease in sensitivity in the long-wavelength region of the spectrum ($\lambda_{0.5} = 3.05\,\mu$m) [8]. The low EL intensity near $\lambda = 3\,\mu$m allowed us to carry out changes in the spatial distribution of the EL intensity at high currents through the $p-n$-junction without upgrading the original measurement algorithm of the microscope. It was assumed that the ratio of the EL intensity in the center of the radiation band ($\lambda_c = 4.2\,\mu$m) and away from it ($\lambda \sim 2.9\,\mu$m) in local regions and in the sample as a whole did not change with the change of the diode current. The data obtained were compared with the results of modeling the EL intensity distribution obtained from the calculated current density distribution. Due to the low IQE value, as well as the high degree of absorption of its own radiation in the active layer of $InAsSb_{0.08}$ with a thickness of $7\,\mu$m [7], we neglected the processes of redistribution of radiation inside the chip due to re-emission.

3. Model description

The simulation of the current density distribution $j(x, y)$ was carried out in accordance with the equivalent diode circuit shown in Figure 2. The mesa region was conditionally divided into strips of equal length Δx (the axis x is directed from the edge of the cathode to the edge of the mesa). The area of each mesa element thus allocated was $S_x = w \cdot \Delta x$, where w — the width of the mesa. For each element „S_x“ „vertical“ (relative to the location of Figure 1) and the lateral components of the series resistance R were calculated. At the same time, the vertical resistance was created as follows: 1) by the transition region between the anode and the layer p-InAsSbP (R_a), 2) the layer p-InAsSbP itself (R_p); 3) by the layer n-InAsSb (R_v). These resistances for each element

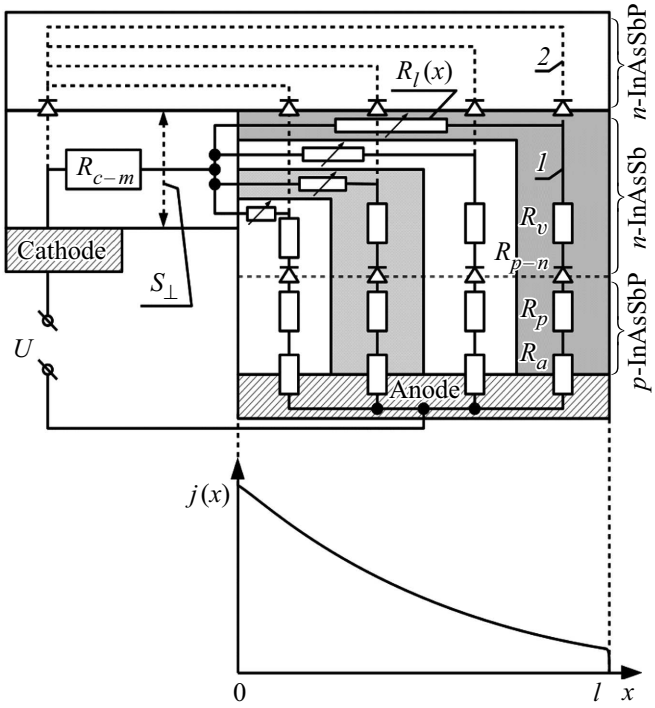

Figure 2. An equivalent diode circuit (top) and a typical view of the current density distribution along the mesa (bottom).

S_x were calculated using the following formulas:

$$R_a = \rho_a/S_x, \quad R_p = \rho_p t_p/S_x, \quad R_v = \rho_n t_n/S_x, \qquad (1)$$

where ρ_a — the specific surface resistance of the transition region between the anode and the layer p-InAsSbP; ρ_p and ρ_n, t_p and t_n — specific volume resistances and layer thicknesses of p-InAsSbP and n-InAsSb, respectively.

According to generally accepted concepts, the electric field lines and, accordingly, the current flow lines do not intersect. This makes it possible to divide the total lateral resistance into elements $R_\ell(x)$, each of which is connected to its own element of $p-n$-junction.

The number of elements was ℓ/Δ_x, where ℓ — the size of the mesa along the axis x (see Figure 2). The cross-sectional area of the element $R_\ell(x)$ was assumed to be equal to $S_\perp \cdot \Delta x/\ell$, where $S_\perp$ — the cross-sectional area of the section of the structure located between the cathode and the mesa (see Figure 1 and 2). The formula for calculating the resistance $R_\ell(x)$ has the form

$$R_\ell(x) = \rho x \ell/(S_\perp \Delta x). \qquad (2)$$

The resistance generated by the n-InAsSbP layer was defined as the geometric sum of the components R_v and $R_\ell(x)$:

$$R_n(x) = \sqrt{[(R_v)^2 + (R_l(x))^2]}. \qquad (3)$$

The total series resistance for the element S_x was determined using the formula

$$R_x(x) = R_a + R_p + R_n(x). \qquad (4)$$

Figure 2 shows that with a forward bias, the current from the anode to the cathode has two possible paths along the axis x: 1) through the narrow-band active layer n-InAsSb and 2) through the wide-band layer n-InAsSbP and the isotypic interface n-InAsSb/n-InAsSbP. In the latter case, the current along the path 2) will be limited due to the energy band discontinuity and the presence of potential barriers on the heteroboundaries [9], similar to the restriction in the DHS samples InAsSbP/InAs/InAsSbP [10]. The passage of current through the wide-band layer n-InAsSbP can be neglected based on this. The $I-V$ characteristics of $p-n$-junction was described by a modified Shockley formula:

$$J = J_o\left[\exp(eU_{p-n}/(\beta kT)) - 1\right], \qquad (5)$$

where J_o — saturation current density, β — ideality factor, U_{p-n} — bias voltage at $p-n$-junction.

The current density distribution $j(x)$ was calculated by solving the following equation for each element S_x

$$j(x)R_x(x)S_x + U_{p-n}(x) = U_1, \qquad (6)$$

where the voltage U_1 was set without taking into account the impact of resistance R_{c-m} (see Figure 2), $U_{p-n}(x)$ — voltage drop at $p-n$-junction in the local area.

The total current in the diode was calculated by summing over all elements:

$$I_{\text{tot}} = \sum j(x)S_x. \qquad (7)$$

The resistance R_{c-m} was determined using the formula

$$R_{c-m} = \rho_c \ell_c w + \rho_n \ell_{c-m}/S_\perp, \qquad (8)$$

where ρ_c — specific surface transition resistance between the cathode and the layer n-InAsSbP, ρ_n — specific volume resistance n-InAsSbP, ℓ_{c-m} the distance from the edge of the cathode to the edge of the mesa (see Figure 1).

The voltage applied to the diode was determined by the formula

$$U = U_1 + I_{\text{tot}}R_{c-m}. \qquad (9)$$

Further, the value of U_1 was adjusted until a satisfactory accordance was obtained between the measured and calculated values of voltage U and current I_{tot} in the diode.

The values of $j(x)$ obtained by solving equation (6) were used to calculate the local values of the concentration of charge carriers $n(x)$. It was assumed that carrier recombination occurred in the active region n-InAsSb via two channels: 1) direct interband radiative recombination and 2) non-radiative Auger recombination. The carrier concentrations $n = n(x)$ were determined by solving the following equation for each element S_x

$$j(x)/(ed) = Bn^2 + Cn^3, \qquad (10)$$

where $n = n(x)$, e — electron charge, d — thickness of the active region n-InAs, B and C — coefficients of radiative and non-radiative Auger recombination, respectively.

The internal quantum efficiency ($\eta_{\text{int}}(x)$) was determined taking into account the values of $n(x)$:

$$\eta_{\text{int}}(x) = (1 + n(x)C/B)^{-1}. \qquad (11)$$

It was also assumed that the radiation output coefficient was the same in all local areas of the active region, i. e. the external quantum output depended only on $\eta_{\text{int}}(x)$. Taking this into account the calculated value of $L(x)$ was assumed to be equal to $L(x) = Bn^2(x)$.

The values of the parameters used in the calculations are given in the table. The recombination coefficients were determined similarly to [6] by the formulas:

$$B = 3.0 \cdot 10^{-10}(E_g/1.5), \qquad (12)$$

$$C = 1.2 \cdot 10^{-27}(E_g^{-2.5})\exp(-4.25E_g), \qquad (13)$$

where $E_g = 0.3$ eV, B — in cm^3/s, C — in cm^6/s.

4. Measurement results and discussion

Figure 3 shows experimental and calculated distributions of the EL intensity $L(x)$, as well as the calculated current density distribution calculated $j(x)$ along the $p-n$-junction for three current values. At a current of 1.6 mA[1]

[1] Measured values $U = 0.048$ V, $I = 1.6$ mA. Calculated values $U = 0.048$ V, $I = 0.94$ mA.

The values of the parameters used for the calculation

Parameter	Value, used in the calculation	Values, given in the literature
The transition resistance between the anode and the layer p-InAsSbP, ρ_a	$1.0 \cdot 10^{-4}$ Ohm $\cdot$ cm^2	$(0.9-1.0) \cdot 10^{-4}$ Ohm $\cdot$ cm^2 [10]
Resistivity of the layer p-InAsSbP, ρ_p	0.065 Ohm $\cdot$ cm	0.01–0.125 Ohm $\cdot$ cm ([10], calculation based on [11] data)
Resistivity of layers n-InAsSb and n-InAsSbP, ρ_n	$5.0 \cdot 10^{-3}$ Ohm $\cdot$ cm	10^{-3}–10^{-2} Ohm $\cdot$ cm ([10], calculation based on data [11])
The transition resistance between the cathode and the layer n-InAsSbP, ρ_c	$3.0 \cdot 10^{-5}$ Ohm $\cdot$ cm^2	$3.7 \cdot 10^{-5}$ Ohm $\cdot$ cm^2 [10]
Saturation current density p–n-junction, j_{sat}	0.5 A/cm^2	0.14–0.32 A/cm^2 [10] $\sim$ 1 A/cm^2 [12]
The ideality factor of the I–V characteristics of p–n-junction, β	1.0	1.37 [10]
Radiative recombination coefficient, B	$1.20 \cdot 10^{-11}$ cm^3/s	$1.1 \cdot 10^{-10}$ cm^3/s [13] $5 \cdot 10^{-11}$ cm^3/s [14]
Auger recombination coefficient, C	$6.80 \cdot 10^{-27}$ cm^6/s	$2.2 \cdot 10^{-27}$ cm^6/s [13] $5 \cdot 10^{-27}$ cm^6/s [14]

(Figure 3, *a*) the normalized calculated values of $L(x)$ and $j(x)$ are close to each other and to the measured distribution of $L(x)$ along the entire mesa. The value of $\eta_{\text{int}}(x)$, according to the calculation (see the insert in Figure 3, *a*), in the mesa regions furthest from the cathode was $\eta_{\max} \sim$ 10% (current density $j_{min}(x) = 1.64$ A/cm^2 at $x = 220\,\mu$m) and as it approached the cathode decreased to $\eta_{\min} \sim 9\%$ ($j_{\max} = 2.35$ A/cm^2 at $x = 0$). The ratio of local EL intensity values $L_{\max}$ in the mesa region closest to the cathode edge to $L_{\min}$ in the mesa region furthest from the cathode edge was $L_{\max}/L_{\min} \sim 1.2$; the corresponding ratio of local current density values $j_{\max}/j_{\min} \sim 1.4$. At the same time, it is obvious that the assumption of direct proportionality between the local values of the EL intensity and the current density, i.e. $L(x) \propto j(x)$, is fulfilled with sufficient accuracy.

At a current of 6.4 mA[2] (Figure 3, *b*) there is a significant difference between the calculated distributions $L(x)$ and $j(x)$. At the same time, the first agrees satisfactorily, and the second significantly diverges from experimental data. The value of $\eta_{\text{int}}(x)$ was $\eta_{\max} \sim 6.4\%$ in „distant“ mesa regions ($x = 220\,\mu$m, $j_{\min} = 7.07$ A/cm^2) and gradually decreased to $\eta_{\min} \sim 4.4\%$ in the mesa region closest to the cathode ($x = 0$, $j_{\max} = 22.6$ A/cm^2, see the insert in Figure 3, *b*). The ratio of the maximum and minimum local values of the EL intensity was $L_{\max}/L_{\min} \sim 2$, and the corresponding ratio of current densities was $j_{\max}/j_{min} \sim 3$. The assumption $L(x) \propto j(x)$, apparently, can still be fulfilled with acceptable accuracy.

At a current of 64 mA[3] (Figure 3, *c*) calculated values $L(x)$ correspond to experimental values only for „distant“ areas of the mesa. For the „of the middle“ part of the mesa, the calculated values of $L(x)$ are significantly lower than the experimental ones. This is most likely due to the imperfection of the model, which does not take into account the features of the output of radiation from different regions of the mesa. When moving away from the edge of the mesa near the cathode, the current density $j(x)$ decreases significantly faster than the EL intensity $L(x)$. The value of $\eta_{\text{int}}(x)$ varied from $\eta_{\max} \sim 3.5\%$ in „distant“ mesa regions ($x = 220\,\mu$m, $j_{\min} = 44.1$ A/cm^2) up to $\eta_{\min} \sim 1.5\%$ in the regions closest to the cathode ($x = 0$, $j_{\max} = 618$ A/cm^2, see the insert in Figure 3, *c*). The ratio of the maximum and minimum local values of the EL intensity was $L_{\max}/L_{\min} \sim 5$, and the corresponding ratio of current densities was $j_{\max}/j_{\min} \sim 10$. The assumption $L(x) \propto j(x)$ is obviously no longer strictly fulfilled. One of the possible reasons for the discrepancy between the calculated and experimental values of the EL intensity ($L(x)$) is the unevenness of the current heating along the sample. It is quite natural to expect that the regions with increased current density, i.e. at $x \sim 0$ in Figure 1 and 3, have a higher temperature than the regions removed from the cathode ($x \sim 200\,\mu$m). An increase in temperature in the InAsSb semiconductor solid solution reduces its internal quantum yield and „shifts“ the EL spectrum to the region of large wavelengths, therefore, in our case, the calculated dependence of $L(x)$ near the overheated region/region with increased current density ($x \sim 0$–$100\,\mu$m) turns out to be sharper than the experimental dependence. On the other hand, the heated area should be larger than the transverse size of the mesa due to the lateral spreading of heat; Figure 3 shows that the low (identical) intensity of (thermal) radiation near the two edges of the mesa ($x \sim -0.1$ mm and $x \sim 0.2$ mm) does not allow concluding that there is a significant temperature gradient dT/dx along the sample. At the moment, this makes it difficult to conduct

[2] Measured values $U = 0.118$ V, $I = 6.4$ mA. Calculated values $U = 0.118$ B, $I = 5.5$ mA.

[3] Measured values $U = 0.48$ V, $I = 64$ mA. Calculated values $U = 0.48$ V, $I = 62.5$ mA.

a more detailed analysis of the data obtained, taking into account the dependence of the spectrum of EL and η_{int} on temperature.

Figure 4 shows the calculated dependence of the internal quantum output on the current density $\eta_{int}(j)$. The value of η_{int} decreased from 10% at $j = 1.64\,A/cm^2$ to 1.5% at $j = 618\,A/cm^2$ with increasing current density according to

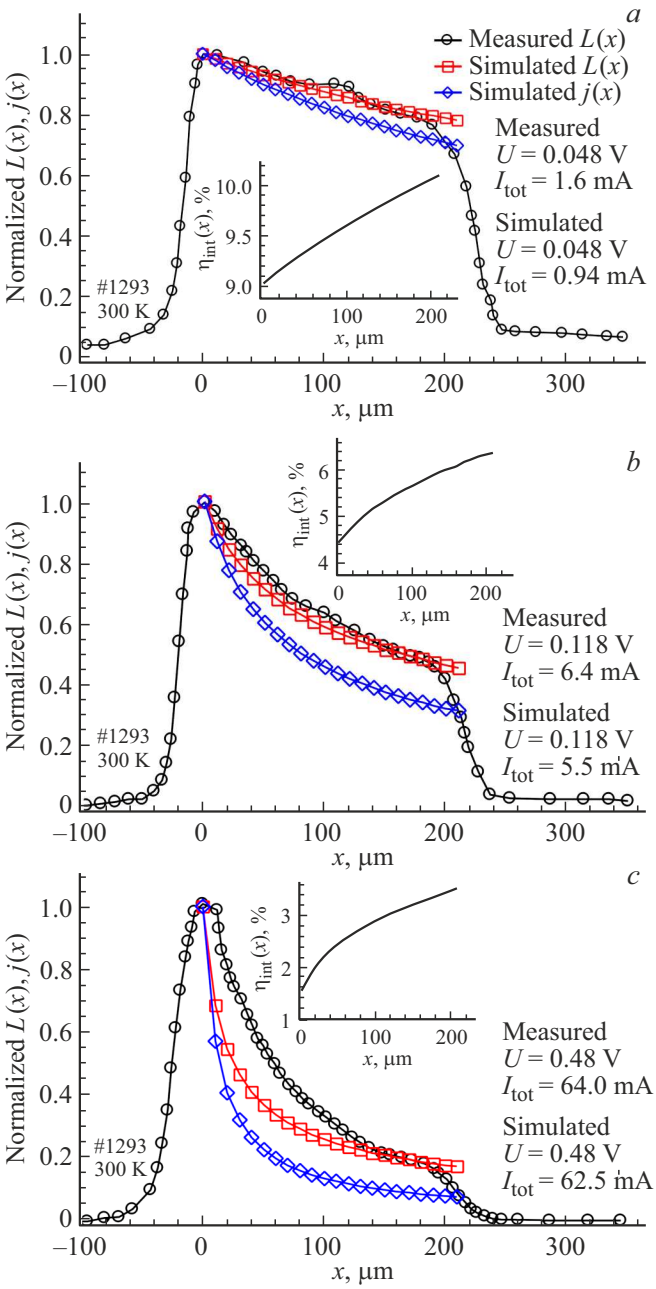

Figure 3. Normalized experimental (Measured) and calculated (Simulated) distributions of EL intensity $L(x)$, calculated current density distributions $j(x)$ over the surface of the diode at currents 1.6 (a), 6.4 (b) and 64 mA (c). The coordinate $x = 0$ corresponds to the edge of the anode closest to the cathode; the axis x is perpendicular to this edge and passes through the center of the mesa. On inserts — calculated distribution of the internal quantum yield of EL (IQE) along the mesa.

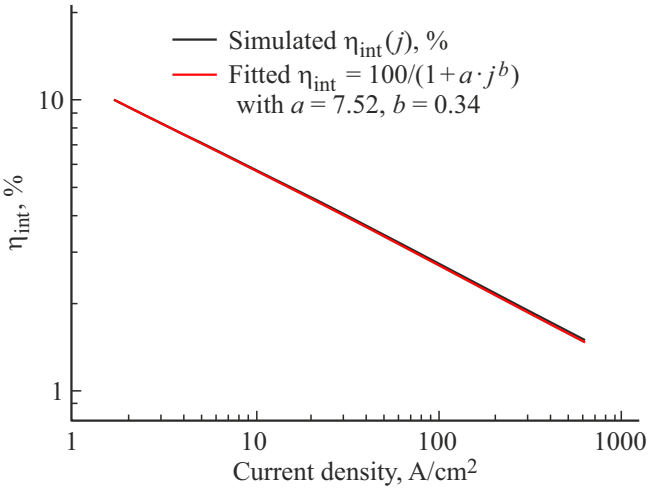

Figure 4. Calculated dependence of the internal quantum efficiency (IQE) on the current density j.

the following dependence:

$$\eta_{int}(j) = (1 + a\,j^b)^{-1}, \qquad (14)$$

where the approximation parameters are $a = 7.52$ and $b = 0.34$. The obtained estimates of the value of the internal quantum yield are close to the calculated values given in the work [6], while it is important to note that when determining it, no assumptions were made about the value of the radiation output coefficient from the sample — one of the main sources of errors in determining the internal quantum efficiency from the measurements of the output power of LED.

5. Conclusion

Thus, it is shown that the internal quantum efficiency of the EL can be estimated by comparing its spatial distribution in samples with current localization with calculated data without taking into account the coefficient of radiation output from the sample. In diodes based on double heterostructures InAsSbP/InAsSb$_{0.08}$ ($\lambda_c = 4.2\,\mu$m), the internal quantum efficiency at 300 K is $\eta_{int} \sim 10\%$ at current density $j \sim 1\,A/cm^2$ and decreases to $\eta_{int} \sim 1.5\%$ at $j \sim 600\,A/cm^2$, which is important to consider when designing LED.

Acknowledgments

The authors would like to thank colleagues from the Mid-IR Diode Optopair Group (MIRDOG) of the Laboratory of Infrared Optoelectronics of the Ioffe Institute of Physics and Technology and employees of „IoffeLED“ LLC, who provided invaluable assistance in the manufacture of samples and conducting experiments.

The near field of self-emission of LEDs was studied in the common use center „Element base of radiophotonics and nanoelectronics: technology, diagnostics, metrology".

Conflict of interest

The authors declare that they have no conflict of interest.

References

[1] A.V. Zagnitko, I.D. Matsukov, V.V. Pimenov, C.E. Salnikov, D.Yu. Fedin, V.I. Alekseev, S.M. Velmakin. ZhTF, **92** (6), 783 (2022). (in Russian).
[2] V.M. Kabatsiy, B.Ya. Khom'yak, O.Yu. Pytovka, Yu.I. Fordzyun. Oswita i nauka, vip. 2 (27), ch. 2. 7 (2019). http://msu.edu.ua/UDC 662.767.1=161.1. Doi:10.31339/2617-0833-2019-2(27)-2-7-12
[3] L. Ch'ien, Y. Wang, A. Shi, X. Wang, J. Bai, L. Wang, F. Li. Infr. Phys. Technol., **108**, 103335 (2020). https://doi.org/10.1016/j.infrared.2020.103335
[4] A.L. Zakgheim. *Svetodiody i ih effektivnoe primenenie* (M. Svetotekhnika, 2021). ISBN 978-5-6043163-4-4
[5] F. Schubert. Svetodiody, translated from English/Ed. by A.E. Yunovich. 2-e izd. (M., Fizmatlit, 2008). (in Russian). ISBN 978-5-9221-0851-5
[6] Ya.Ya. Kudrik, A.V. Zinovchuk. Pisma ZhTF, **38** (10), 14 (2012). (in Russian).
[7] A.A. Klimov, M.A. Remenny. *Tez. dokl. „Nedelya nauki SPbPU": mater. scientific. conf. s mezhdunar. uchastiem* (19–24 November 2018 g.), Luchshie dokl. (St. Petersburg, Polytech-press, 2018) p. 150 (in Russian).
[8] V.M. Bazovkin, A.A. Guzev, A.P. Kovchavtsev, G.L. Kuryshev, A.S. Larshin, V.G. Polovinkin. Prikl. fizika, № 2, 97 (2005). (in Russian).
[9] N.L. Bazhenov, K.D. Mynbayev, A.A. Semakova, G.G. Zegrya. FTP, **56** (5), 479 (2022). (in Russian).
[10] B.A. Matveev, V.I. Ratushnyi, A.Yu. Rybal'chenko. Techn. Phys., **65** (5), 799 (2020). DOI: 10.1134/S1063784220050187
[11] T.I. Voronina, T.S. Lagunova, K.D. Moiseev, A.E. Rozov, M.A. Sipovskaya, M.V. Stepanov, V.V. Sherstnev, Yu.P. Yakovlev. FTP, **33** (7), 781 (1999). (in Russian).
[12] P. Chakrabarti, A. Krier, X.L. Huang, P. Fenge. IEEE Electron Dev. Lett., **25** (5), 283 (2004).
[13] New Semiconductor Materials. Biology systems. Characteristics and Properties. www.matprop.ru
[14] M. Carras, G. Marre, B. Vinter, J.L. Reverchon, V. Berger. Design and fabrication of InAsSb detectors. *Detectors and Associated Signal Processing* (Saint Etienne, France, 19 February, 2004). Proc. SPIE, 5251. https://doi.org/10.1117/12.514204

Translated by A.Akhtyamov